Towards graphene-based quantum interference devices

J. Munárriz,[1] F. Domínguez-Adame[1] and A. V. Malyshev[1,2]

[1] GISC, Departamento de Física de Materiales, Universidad Complutense, E-28040 Madrid, Spain

[2] Ioffe Physical-Technical Institute, St-Petersburg, Russia

Abstract.

A new type of quantum interference device based on a graphene nanoring in which all edges are of the same type is studied theoretically. The superposition of the electron wavefunction propagating from the source to the drain along the two arms of the nanoring gives rise to interesting interference effects. We show that a side-gate voltage applied across the ring allows for control of the interference pattern at the drain. The electron current between the two leads can therefore be modulated by the side gate. The latter manifests itself as conductance oscillations as a function of the gate voltage. We study quantum nanorings with two edge types (zigzag or armchair) and argue that the armchair type is more advantageous for applications. We demonstrate finally that our proposed device operates as a quantum interference transistor with high on/off ratio.

PACS numbers: 72.80.Vp;73.22.Dj;73.22.-f

Nanotechnology ***22****, 365201 (2011)*

1. Introduction

Graphene is a promising candidate for replacing semiconductors as the basic material for the design of new nanodevices due to its truly two-dimensional geometry as well as large carrier mobility [1]. Low-energy electronic excitations in graphene can be described by the Dirac Hamiltonian for massless particles [2]. It is well established that the Dirac equation leads to the so-called Klein tunneling [3]. In graphene Klein tunneling manifests itself as the occurrence of perfect transparency of barriers at normal incidence, as predicted by Katsnelson *et al.* [4] and observed in experiments later [5]. This peculiar tunneling would lead to undesired charge leakage in graphene-based devices. While in particle physics it is known that there exist relativistic interactions for which Klein tunneling is absent [6, 7], it seems that they have no counterpart in graphene and confining electrons is a challenging task while being necessary for many applications. Therefore, a significant amount of effort has been focused on graphene-based nanodevices that could enhance carrier confinement, such as p–n junctions [8, 9], superlattices [10–12] and field effect transistors (FET) [13, 14].

Interference effects of coherent electron transport through graphene nanorings open an alternative possibility of controlling quantum transport without relying on potential barriers. Interference effects in graphene subjected to a perpendicular magnetic field, such as current revivals [15] or Aharonov-Bohm conductance oscillations in ring-shaped devices [16–20], have already been studied. In particular, in Ref. [18] it was pointed out that these conductance oscillations are robust under the effects of either edge or bulk disorder. Wu *et al.* [19] investigated quantum transport through a graphene nanoring theoretically and concluded that the device behaves like a resonant tunneling one, in which the resonance energy can be tuned by varying the size of the device or the external magnetic field. Effects of an electrostatic potential applied to one of the arms on the Aharonov-Bohm magnetoconductance were discussed in Ref. [20].

In contrast to previous studies of magnetically induced interference effects [16–19], in this work we consider a new design of graphene interference device in which electron transport is controlled *without* applying a magnetic field. We demonstrate that charge carrier transport can be tuned instead by applying a side-gate voltage across a graphene nanoring. We show that in this case the relative phase of the electron wave function in the two arms can be varied, leading to a constructive or destructive interference at the drain, which results in conductance oscillations and current modulation.

2. System and modeling

The studied system comprises a graphene nanoring with 60° turns attached to semi-infinite leads. The schematic diagram of the device is shown in figure 1. The total length of the ring is L, its total width is W while the width of all nanoribbons is w. It is known that the dispersion relation of a quasi-one-dimensional graphene nanoribbon is drastically different from that of a two-dimensional sheet of this material [21]. In

particular, the electronic structure of the nanoribbon is very sensitive to the type of edges [22]. Thus, if a nanoribbon has a turn which does not preserve the edge type, a propagating charge carrier would experience strong scattering at the turn due to the electronic structure mismatch, which is disadvantageous for transport. We propose therefore the above mentioned design of the quantum nanoring with 60° turns, which does preserve the edge type and greatly reduces such scattering at the turns. According to recent studies [23], atomic-scale precision along the edges can be experimentally achieved, which can facilitate the fabrication of the proposed device.

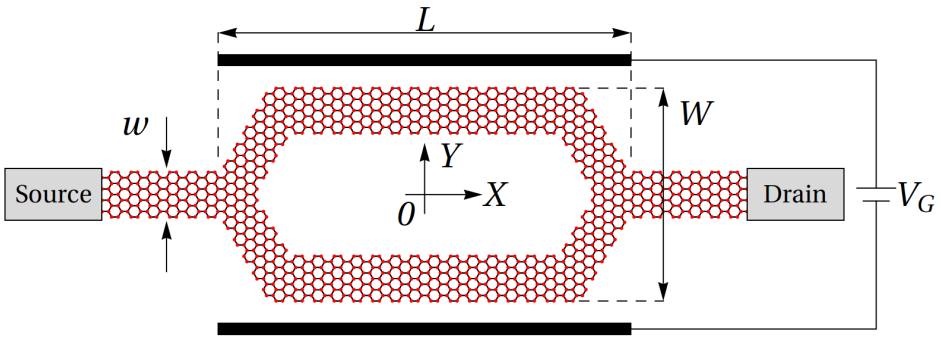

Figure 1. Schematic diagram of the device: a graphene nanoring attached to two leads. The geometry is determined by the parameters L, W, and w. The side-gate voltage V_G is applied across the nanoring as shown in the plot. A back-gate voltage can also be applied to shift the Fermi level.

To model our device, we consider the following tight-binding Hamiltonian describing the motion of a single electron in graphene

$$\mathcal{H} = \sum_i \epsilon_i \mid i \rangle\langle i \mid + \sum_{\langle i,j \rangle} V_{ij} \mid i \rangle\langle j \mid , \tag{1}$$

where the second sum is restricted to nearest neighbors. Hereafter we use the simplest model and assume that the graphene lattice is undistorted, so we take $V_{ij} = -t$ with $t = 2.8\,\mathrm{eV}$ [1], and neglect all spin-related effects (see, *e. g.*, Refs. [24, 25] or Ref. [26] for a review). The site energy ϵ_i can depend on the position of the i-th atom due to the presence of the source-drain (SD) and both back-gate and side-gate voltages. The profile of the electric field can be calculated by solving the Poisson and Schrödinger equations self-consistently. However, for simplicity, we assume a simplified side-gate potential profile: it is linear in the y direction ($|y| < W/2$) while in the x direction it is (i) constant within the nanoring area ($|x| \le L/2$), and (ii) it decays exponentially towards the two leads (for $|x| \ge L/2$).

Using the transmitting quantum boundary method [27, 28] for each energy E and gate voltage V_G we obtain the wave function in the whole sample and the transmission coefficient $T(V_G, E)$. Using the latter we can calculate the current-voltage characteristics. We performed numerical simulations for nanorings of a variety of sizes, geometries and both possible types of edges: zigzag and armchair (see insets in figure 2). We found that these two types of edges result in very different transmission

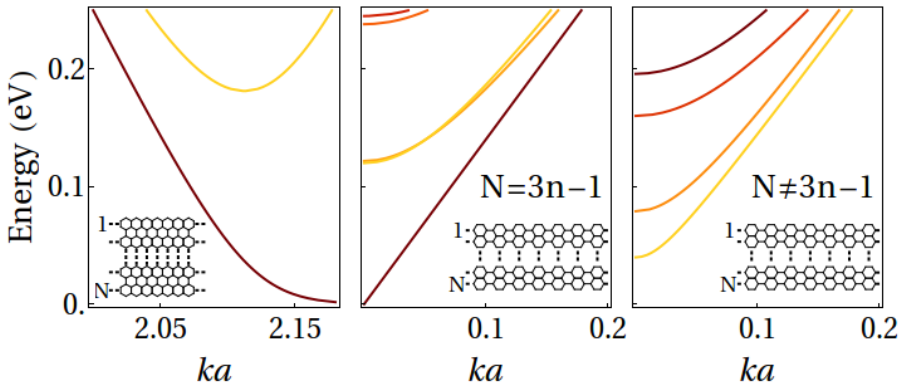

Figure 2. Dispersion relations calculated for three different nanoribbons: A nanoribbon with zigzag edges and $N = 70$ (left panel) and nanoribbons with armchair edges with $N = 62$ and $N = 63$ (middle and right panels, respectively). The insets show the corresponding atomic arrangement of each nanoribbon.

coefficient patterns. These patterns are intimately related to the dispersion relation in the nanoribbons forming the sample. It has been demonstrated that carbon atoms at graphene edges undergo considerable reconstruction [22] which changes the energy dispersion close to the Dirac point. The states which are more affected by such a reconstruction are edge states. Those, however, are not very promising from the point of view of electronic transport because, being quasi-one-dimensional sates, they will also be strongly affected by edge disorder and become localized. The more usual states have low electron density at the edges and will therefore not see themselves affected so much by neither the edge reconstruction nor the edge disorder. We will focus primarily on the latter states and neglect therefore all reconstruction related effects. In figure 2 we present the energy dispersion relations calculated for infinite nanoribbons. The transverse wavenumber k is measured from the Dirac point in units of the inverse lattice spacing a^{-1} along the nanoribbon (i. e $a = \sqrt{3}\,a_0$ for zigzag edges and $a = 3\,a_0$ for armchair ones, where $a_0 \approx 1.4\,\text{Å}$ is the interatomic distance). The left panel shows the dispersion in the case of a zigzag edged nanoribbon. The dispersion is gapless, with low-energy excitations corresponding to high wave numbers k. For a symmetric nanoribbon with armchair edges the energy spectrum depends on the number N of hexagons per wider nanoribbon slice [22]. If $N \neq 3n - 1$ where n is a positive integer, the spectrum is gapless and linear for small k (see the middle panel), otherwise the dispersion has a gap at $k = 0$ and it is quadratic in the vicinity of this point, as can be seen in the right panel. Such an energy spectrum is typical for conventional semiconductors. As we show below, the latter configuration presents more robust and promising transmission patterns for transport control and applications. In all three cases, when the ribbon width is increased consecutive dispersion branches become closer to each other and the energy region with a small number of propagating eigenmodes shrinks. Because we are interested in interference related effects we will be focusing on the one-mode regime in

which these effects are not smeared out due to the superposition of several modes.

3. Transmission coefficient: Resonance bands

The sample that we address in this section has armchair edges and the following geometry: $L = 214\,\text{nm}$, $W = 107\,\text{nm}$ and $w = 15.1\,\text{nm}$ (which corresponds to $N = 62$). In figure 3 we show the transmission coefficient as a function of the Fermi energy and side-gate voltage V_G. The transmission pattern consists of a series of very sharp and narrow resonance lines. Outside the resonances the transmission is vanishingly small. To illustrate this more clearly we show cross sections of the transmission map taken along the horizontal red and vertical blue lines in the upper panel of figure 3, which corresponds to $V_G = 0$ (lower left panel) and $E = 19.2\,\text{meV}$ respectively (lower right panel). We checked that the wavefunction of a high transmission state (not shown here) has a huge pile up in the region of the nanoring, which is the typical wavefunction structure of a resonance state. We note that such a wavefunction is always localized in only one arm of the nanoring.

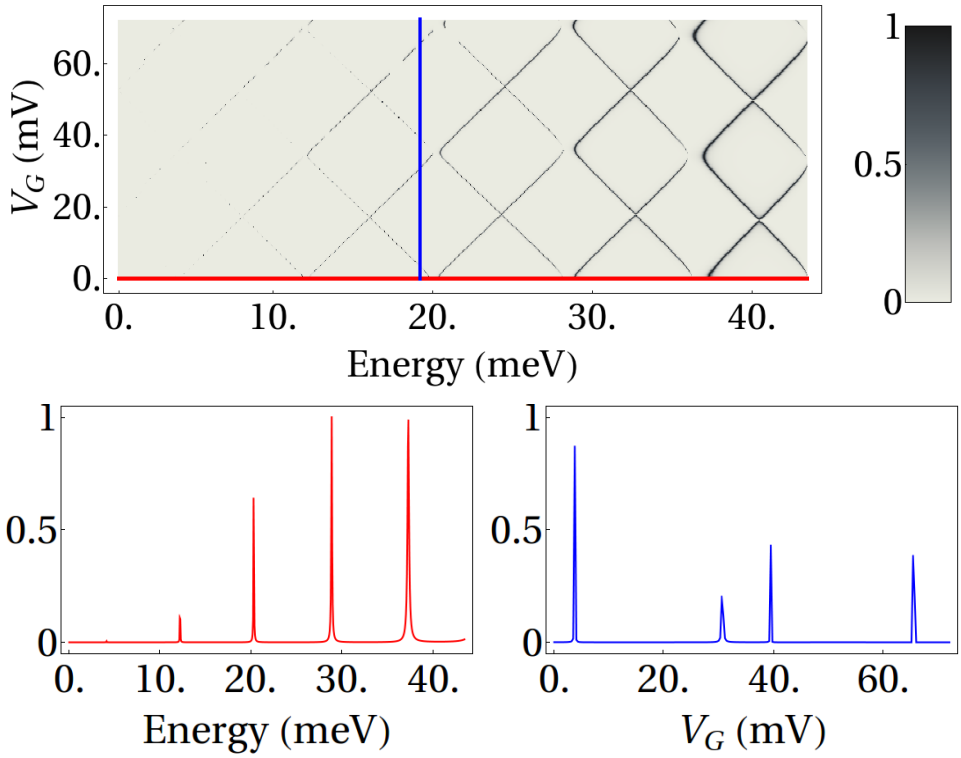

Figure 3. The upper panel shows the transmission map for a system with armchair edges and $N = 62$, as a function of the Fermi energy E and the gate voltage V_G. Lower left and right panels show a cross section of the transmission map along the horizontal red and vertical blue lines in the upper plot, corresponding to $V_G = 0$ and $E = 19.2\,\text{meV}$, respectively.

Although in the vicinity of a resonance the transmission can be changed abruptly by a very small variation of the side-gate voltage, which could be very attractive for

applications, this type of device can hardly be practical because the resonances are very narrow and can easily be affected by perturbations, such as disorder. Our calculations confirmed this conjecture.

The straight lines observed in the maps shown in figure 3 can easily be understood using the following reasoning. The effect of the transverse electric field can be seen as a shift in energy in the upper and lower arms of the nanoring. Therefore, if a side-gate voltage V_G is applied, then the energy shifts in the upper and lower arms can be estimated as $+V_G\,\widetilde{W}/2$ and $-V_G\,\widetilde{W}/2$, respectively. Here $\widetilde{W}$ is some effective width of the nanoring. Therefore, an incoming mode with wave vector $k(E_{\rm in})$ will propagate through the upper branch with a wave vector $k(E_{\rm in}+V_G\,\widetilde{W}/2)$ and with $k(E_{\rm in}-V_G\,\widetilde{W}/2)$ in the lower one. If the resonance condition without transverse field is obtained at $E_{\rm res}$, then when a small voltage is applied, there will be resonances at $E_{\rm res}\pm V_G\,\widetilde{W}/2$. When the dispersion relation is linear or almost linear, this condition leads to the occurrence of the observed straight lines crossing at $V_G = 0$ in the transmission map. To check the validity of this simplified picture we calculated the transmission for a system with one single arm, which resulted in the same transmission map but without the lines corresponding to resonances of the removed branch.

4. Transmission coefficient: Interference induced bands

We now turn to the most promising configuration: a nanoring composed of nanoribbons with armchair edges and $N = 3n - 1$ (n being a positive integer) for which the energy spectrum has a gap at the Dirac point. The dispersion relation in this case is parabolic in the vicinity of $k = 0$ (see right panel of figure 2), which makes it similar to conventional semiconductor. The energy gap decreases as the nanoribbon width increases. The transmission coefficient presented in figure 4 manifests two regions: at lower Fermi energies the aforementioned resonant behaviour with very narrow peaks is observed while at higher energies the transmission comprises wider bands. As we show below these bands arise from interference effects. The lower right plot in figure 4 shows the dependence of the transmission coefficient on the gate voltage for a fixed Fermi energy (it corresponds to the cross section of the transmission map along the vertical blue line in the upper panel). Similar plots are obtained for other higher Fermi energies, as long as only one single mode contributes to the transmission.

In order to study the nature of these wider bands we plot the real part of the envelope wavefunction for the three energies marked by open circles and letter A, B and C in the lower right panel of figure 4. The system has high transmission for the first and the last energy values (denoted A and C); the corresponding wavefunctions manifest a clear constructive interference patterns at the right lead (upper and lower panels of figure 5). Contrary to that, as the middle panel suggests, the two parts of the low transmission state B are propagating along the two branches of the nanoring in such a way that they arrive to the right extreme of the nanoring being out of phase with each other, which gives rise to destructive interference at the drain and practically

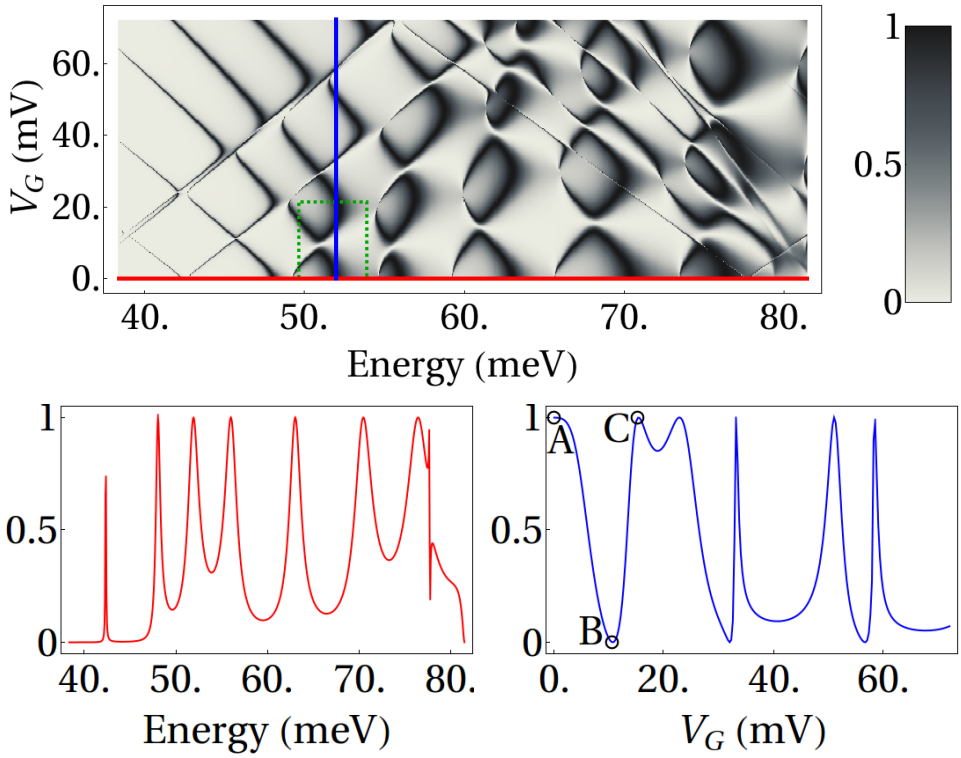

Figure 4. Same as in the figure 3 but for $N = 63$ and $E = 51.9\,\text{meV}$. The green dashed square shows the region used to calculate the current-voltage characteristics in section 6. In the lower right panel we mark the first two maxima and the first minimum. The corresponding wavefunctions are plotted in figure 5.

zero transmission coefficient. Similar patterns are obtained for all other extrema in this higher Fermi energy region.

We note that these interference induced bands are much wider than those having resonance nature and therefore we expect them to be more robust and stable with respect to perturbations, such as disorder. Effects of disorder will be discussed in the next section, where we show that such a conformation of the nanoribbons comprising the nanoring is the most favorable for applications.

For completeness, we address the sample with zigzag edges; the conforming nanoribbons have a width of $w = 15\,\text{nm}$ ($N = 70$). Other geometrical parameters are as follows: $L = 150\,\text{nm}$ and $W = 102\,\text{nm}$. Such a nanoribbon has a gapless dispersion relation, with low-energy excitations corresponding to high wave numbers k (see left panel of figure 2). Similar to the previous case of the armchair edged sample, the transmission map also presents interference bands (see figure 6). However, these bands are considerably narrower than in the case of the armchair edges, which makes them less robust under perturbations and, presumably, less suitable for applications.

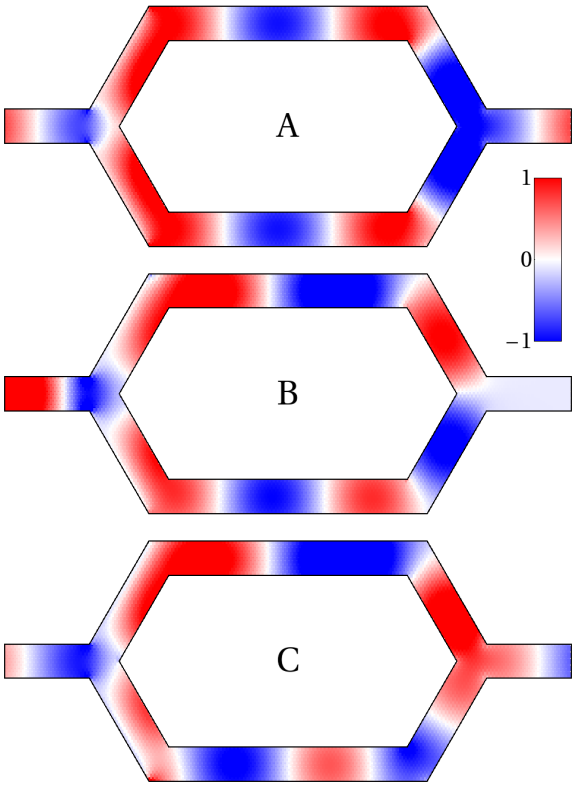

Figure 5. Real part of the envelope wavefunction corresponding to the three states with different transmission coefficients marked by open circles and labeled A, B and C in the lower right panel of figure 4.

5. Effects of the edge disorder

In this section we address the effects of the edge disorder on the transport properties of the proposed device. We take the second sample with armchair edges to study these effects. To do so, we remove pairs of carbon atoms from the edges with some given probability p. By removing pairs rather than individual atoms we assure that there are no dangling atoms in the sample, so we do not have to deal with complicated edge reconstruction effects. The transmission coefficient calculated for one particular realization of disorder for $p = 0.05$ and zero side-gate voltage is presented in figure 7. Dashed line with blue filling represents the transmission coefficient of an ordered sample, while the solid line that of the disordered one. There are two important trends that can be observed. First, the transmission bands in the latter case are shifted to higher energies with respect to their positions in the regular sample. This is due to the fact that we were removing the atoms from the edges of the nanoribbons, making them effectively narrower, which leads to higher quantization energy in the lateral direction. Second, one can observe the appearance of anti-resonances in the bands. We attribute those to the edge states localized by the disorder. Such discrete states lie at the continuum of band states. Mixing between a discrete state and one belonging to the continuum

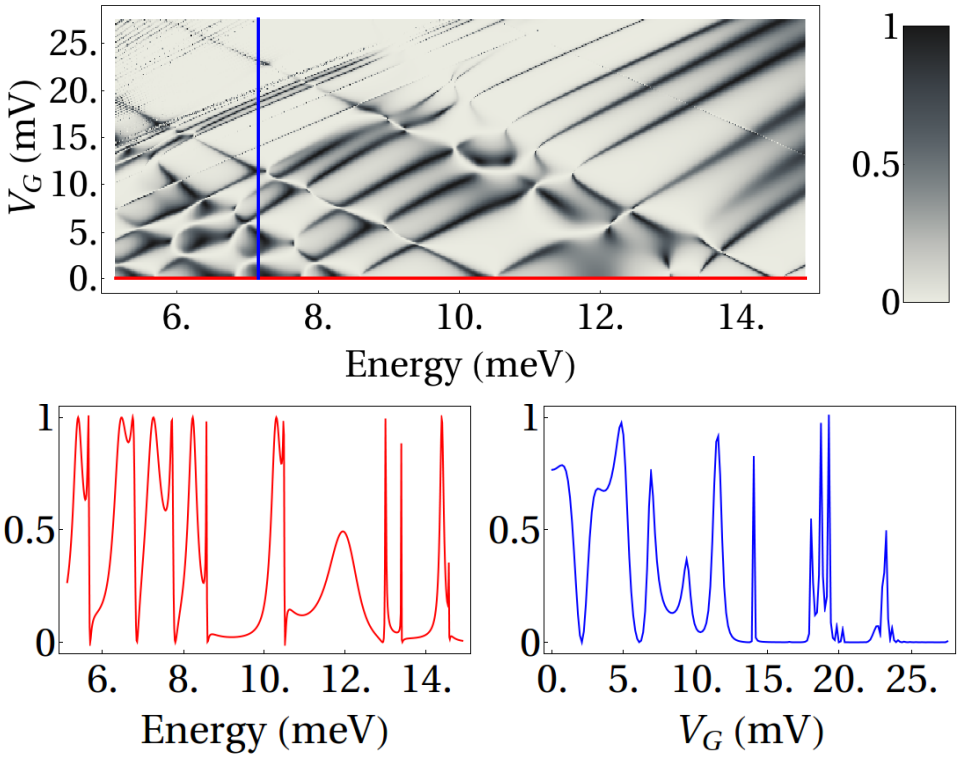

Figure 6. Same as in figure 3 but for zigzag edges and $N = 70$.

gives rise to the typical Fano resonance [29, 30]. The most important finding is that transmission bands are not destroyed by the moderate disorder, so we conclude that such a device (with armchair edges and gaped spectrum) is robust under perturbations. Our calculations confirm that nanorings having different configurations (zigzag edges or armchair edges with linear dispersion) are affected by the disorder to a much larger extent.

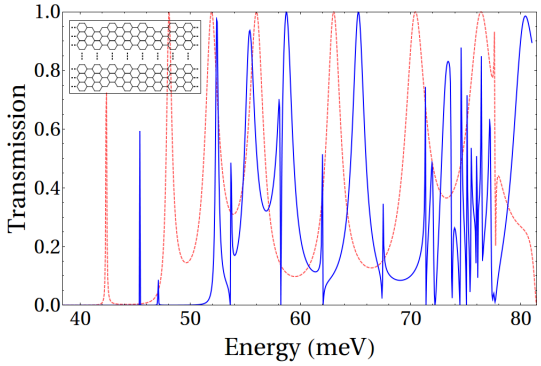

Figure 7. Transmission coefficient of the ordered sample (same red line as the one plotted in the lower left panel of figure 4) and a disordered one (blue line). The inset shows a typical disorder realization.

6. Current-voltage characteristics

In this section we address current-voltage characteristics of the device with armchair edges and gaped spectrum. In order to calculate transport properties of the device, the Landauer-Büttiker scattering formalism is used. The current flowing through the device can be calculated as follows [31, 32]

$$I = \frac{2e}{h} \int T(V_G, E) \, [\, f_l(E, V_{SD}) - f_r(E, V_{SD}) \,] \, dE \, , \tag{2}$$

where the Fermi functions of the left and right contacts are given by $f_l(E, V_{SD}) = [1 + \exp{(E_F - E)/kT}]^{-1}$ and $f_r(E, V_{SD}) = [1 + \exp{(E_F - eV_{SD} - E)/kT}]^{-1}$ respectively, V_{SD} is the SD voltage applied across the whole sample in the x direction, and E_F is the Fermi energy at equilibrium, the position of which can be controlled by the back-gate voltage. The temperature T is set to $4K$. The $I - V$ characteristics were calculated within the region of the SD and gate voltages marked with the dashed green rectangle in figure 4. We assume here that the Fermi energy of both contacts is set to the working point by the back-gate voltage: to the energy E_S (corresponding to the left edge of the rectangle) and then the SD voltage is changed within the selected window.

The corresponding $I - V$ characteristic is presented in figure 8. The upper panel shows the complete $I(V_G, V_{SD})$ surface. As can be seen from the figure, the side-gate voltage can be used to control the current through the device. The lower panel of the figure shows the dependence of the current on the side-gate voltage V_G for several fixed values of SD voltage (specified in the legend). Note that the on/off ratio of this quantum interference transistor can be as high as about 10. It should be stressed that the current-voltage dependencies typical for a traditional FET are monotonous functions of the gate voltage. However, our proposed device manifests more interesting gate voltage dependence. In particular, the $I - V$ curves have negative differential resistance parts, which can be very useful for applications. Another underlying difference between a traditional FET and the proposed device is the principle of operation. In the latter case it is based upon an essentially quantum mechanical effect: the interference between the two paths of the wavefunction propagating along the two arms of the nanoring.

Several designs of nanodevices based on single organic molecules exploiting various quantum mechanical effects have already been put forward (see, e. g. Refs. [33, 34] and references therein). In particular, Stafford *et al.* studied quantum interference effects in aromatic molecules to modulate the current flow [33]. More complex organic molecules, such as the DNA, were proposed to design FETs and more sophisticated devices [34]. However, single-molecule electronics often requires almost atomic level control of contacts, it can be affected greatly by vibrations and could be subject to structural instabilities under required voltages. Fabrication of graphene nanorings seems to be more feasible (at least nowadays), and they can also sustain higher voltages and currents, which is advantageous for applications.

Finally, we point out that our proposed device should be operating in the single mode regime in order to use the interference effects in their most pure form. When

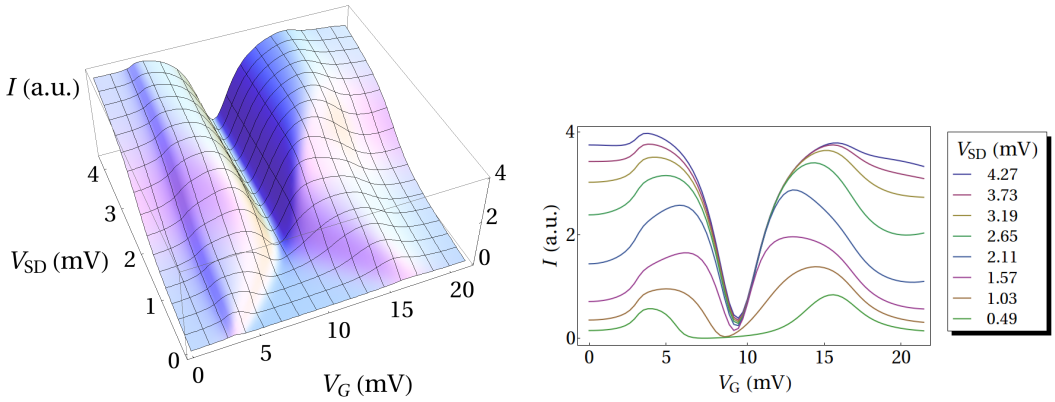

Figure 8. Current-voltage characteristics of the device with armchair edges and the spectrum with a gap.

the second mode comes into play the interference bands smear out and the current control is expected to be less efficient. In this regard, the dispersion relations of the nanoribbons constituting the device provide an important starting point because they allow us to select the appropriate energy window where one single mode is contributing to the transport. For the considered nanoribbon width of about 15 nm such a window is on the order of 40 meV (see right panel of figures 2 and 4). As the width w is increasing the window is shrinking while its lower edge is approaching the Dirac point. On the other hand, electronic transport through wider nanoribbons are less affected by the edge disorder. These considerations should be taken into account when designing and fabricating the real world device.

7. Summary

In summary, we have proposed and studied a new quantum interference device based on a graphene nanoring with 60° turns. Transport properties of the device are sensitive to the type of edges (zigzag or armchair). The ring comprised of nanoribbons with armchair edges and quadratic dispersion with a gap were found to be the most advantageous for electronic transport because the transmission pattern presents wide bands of high transitivity in this case. We showed that the current flow through the device can be controlled by the side-gate voltage. Such a voltage changes the relative phase of the electron wavefunction in the two arms of the ring resulting in constructive or destructive interferences at the drain. Consequently, the current flow can be modulated efficiently without applying a magnetic field, so the device operates as a quantum interference effect transistor. We demonstrated that the predicted transistor effect is robust under moderate edge disorder. We conclude therefore that our proposed devices is a promising candidates for real world technological applications.

This work was supported by MICINN (projects Mosaico and MAT2010-17180). The authors are grateful to P. A. Orellana for useful discussions of the Fano effect.

References

[1] A. H. Castro Neto, F. Guinea, N. M. R. Peres, K. S. Novoselov and A. K. Geim, Rev. Mod. Phys. **81**, 109 (2009).
[2] P. R. Wallace, Phys. Rev. **71**, 622 (1947).
[3] O. Klein, Z. Phys. **53**, 157 (1929).
[4] M. I. Kastnelson, K. S. Novoselov and A. K. Geim, Nat. Phys. **2**, 620 (2006).
[5] N. Stander, B. Huard and D. Goldhaber-Gordon, Phys. Rev. Lett. **102**, 026807 (2009).
[6] S. Ru-keng and Z. Yuhong, J. Phys. A: Math. Gen. **17**, 851 (1984).
[7] F. Domínguez-Adame, Phys. Lett. A **162**, 18 (1992).
[8] J. R. Williams, L. DiCarlo, C. M. Marcus, Science **317**, 638 (2007).
[9] H.-Y. Chiu, V. Perebeinos, Y.-M. Lin and P. Avouris, Nano Lett **10**, 4634 (2010).
[10] C. Bai and X. Zhang, Phys. Rev. B **76**, 075430 (2008).
[11] H. Sevinçli, M. Topsakal and S. Ciraci, Phys. Rev. B **78**, 245402 (2008).
[12] M. Yang, A. Nurbawono, C. Zhang, Y. P. Feng and Ariando, Appl. Phys. Lett. **96**, 193115 (2010).
[13] Xinran Wang, Yijian Ouyang, Xiaolin Li, Hailiang Wang, Jing Guo, and Hongjie Dai, Phys Rev. Lett. **100** 206803 (2008).
[14] Ye Lu, Brett Goldsmith, Douglas R. Strachan, Jong Hsien Lim, Zhengtang Luo, A. T. Charlie Johnson, Small **6**, 2748 (2010).
[15] E. Romera and F. de los Santos, Phys. Rev. B **80** 165416 (2009)
[16] S. Russo, J. B. Oostinga, D. Wehenkel, H. B. Heersche, S. S. Sobhani, L. M. K. Vandersypen and A. F. Morpurgo, Phys. Rev. B **77**, 085413 (2008).
[17] M. Zarenia, J. Milton Pereira, A. Chaves, F. M. Peeters, and G. A. Farias, Phys. Rev. B **81** 045431 (2010)
[18] J. Wurm, M. Wimmer, H. U. Baranger and K. Richter, Semicond. Sci. Technol. **25**, 034003 (2010).
[19] Z. Wu, Z. Z. Zhang, K. Chang and F. M. Peeters, Nanotechnology **21**, 185201 (2010).
[20] J. Schelter, D. Bohr and B. Trauzette, Phys. Rev. B **81**, 195441 (2010).
[21] K. Nakada, M. Fujita, G. Dresselhaus and M. S. Dresselhaus, Phys. Rev. B **54**, 17954 (1996).
[22] Young-Woo Son, Marvin L. Cohen, and Steven G. Louie, Phys. Rev. Lett. **97**, 216803 (2006)
[23] X. Jia *et al*, Science **323**, 1701 (2009).
[24] H. Şahin and R. T. Senger, Phys. Rev. B **78** 205423 (2008)
[25] H. Şahin, R. T. Senger, and S. Ciraci, J. Appl. Phys. **108** 074301 (2010)
[26] Oleg V. Yazyev, Rep. Prog. Phys. **73** 056501 (2010)
[27] C. S. Lent and D. J. Kirkner, J. App. Phys. **67**, 6353 (1990).
[28] D. Z.-Y. Ting, E. T. Yu and T. C. McGill, Phys. Rev. B **45**, 3583 (1992).
[29] U. Fano, Nuovo Cimento **12**, 156 (1935).
[30] I. Gómez, F. Domínguez-Adame and P. Orellana, J. Phys. Condens. Matter **16**, 1613 (2004).
[31] D. K. Ferry and S. M. Goodnick, *Transport in Nanostructures* (Cambridge University Press, 1997)
[32] S. Data, *Electronic Transport in Mesoscopic Systems*, (Cambridge University Press, 2007).
[33] C. A. Stafford, D. M. Cardamone and S. Mazumdar, Nanotechnology **18**, 424014 (2007).
[34] A. V. Malyshev, Phys. Rev. Lett. **98**, 096801 (2007).